The final publication is available at

https://doi.org/10.1016/j.jcat.2021.05.024

Additional Information

Highly Efficient Hydroamination of Phenylacetylenes with Anilines Catalysed by Gold Nanoparticles Embedded in Nanoporous Polymer Matrix: Insight into the Reaction Mechanism by Kinetic and DFT Investigations

Antonella Dentoni Litta,[1][†] Antonio Buonerba,[2][†] Alberto Casu,[3] Andrea Falqui,[3] Carmine Capacchione,[1] Antonio Franconetti,[4] Hermenegildo Garcia[5] and Alfonso Grassi[1][*]

[1] *Department of Chemistry and Biology "Adolfo Zambelli", University of Salerno, Via Giovanni Paolo II, 84084 Fisciano (SA), Italy.*

[2] *Inter-University Centre for Prediction and Prevention of Relevant Hazards (Centro Universitario per la Previsione e Prevenzione Grandi Rischi, C.U.G.RI.) and Sanitary Environmental Engineering Division (SEED), Department of Civil Engineering, University of Salerno, Via Giovanni Paolo II, 84084 Fisciano (SA), Italy.*

[3] *King Abdullah University of Science and Technology (KAUST), Biological and Environmental Sciences and Engineering (BESE) Division, 23955-6900 Thuwal, Saudi Arabia.*

[4] *Departamento de Química Orgánica, Facultad de Química. Universidad de Sevilla. C/ Profesor García González, 1, 41012, Sevilla, Spain*

[5] *Departamento de Quimica and Instituto Universitario de Tecnologia Quimica (CSIC-UPV), Universitat Politecnica de Valencia, Av. De los Naranjos s/n, 46022, Valencia, Spain.*

[†] *These authors equally contributed.*

[*] *E-mail: agrassi@unisa.it.*

Abstract

The synthesis of aromatic ketimines via hydroamination of phenylacetylenes (PAs) with anilines (ANs) has been accomplished in high yields and with excellent regio- and stereo-selectivity using gold nanoparticles (AuNPs) embedded in crystalline syndiotactic polystyrene-*cis*-1,4-polybutadiene (sPSB) multiblock copolymer matrix. The performances of the AuNPs-sPSB catalyst exceed those of the other commercial gold catalysts as a result of the physical chemical properties of the nanoporous polystyrenic support which allows excellent activity, thermal stability and recyclability of the catalyst. Electron donating (EDGs) and electron withdrawing (EWGs) substituents onto the aromatic group of ANs and PAs yield, in all examined cases, high selectivity in the formation of the thermodynamic favoured *E* stereoisomer of the aromatic ketimines. Kinetic investigation of the reaction mechanism in the presence of AN and of the deuterated analogue, AN-*N,N-d$_2$*, highlighted a new reaction pathway for the hydroamination reaction, which was also supported by DFT calculations. Actually, the formation of AN aggregates stabilized by hydrogen bonding interactions produces a favourable transition state for the nucleophilic attack of AN to PA, coordinated/activated onto AuNPs surface. Moreover, an additional AN molecule cooperatively assists the 1,3-hydrogen shuttling from the N atom to the C$_\beta$ of the coordinated enamine intermediate to produce the kinetically favoured *Z*-ketimine intermediate that in turn evolves into the thermodynamically stable *E*-aromatic ketimine. The first order kinetics observed for AN, along with the experimental energetic barrier ($\Delta G^{\ddagger} = 26.6 \pm 0.7$ kcal mol^{-1}; $\Delta H^{\ddagger} = 13.4 \pm 1.8$ kcal mol^{-1}; $\Delta S^{\ddagger} = -0.04 \pm 0.04$ kcal mol^{-1} K^{-1}) found in good agreement with the energy of the transition state calculated for the 1,3-hydrogen shift in the DFT modelling, strongly support that the latter is the rate determining step in the gold catalysed hydroamination of AN with PA.

Keywords

Hydroamination; gold nanoparticles; nanoporous polymer support; reaction kinetics; DFT modelling.

1. Introduction

Nitrogen-containing organic compounds find wide application in the synthesis of fine chemicals, polymers, solvents, surfactants and pharmaceuticals.[1-6] The development of new methodologies for the synthesis of amines and imines, or heterocyclic compounds such as indoles and quinolones, from accessible and low cost reagents, is in the focus of research interests in organic, pharmaceutical and industrial chemistry.[1-6] In this contest, hydroamination of alkenes and alkynes is a convenient synthetic route because it is one the most cost-effective processes, showing high efficiency and sustainability because of the 100% atom economy of the reaction.[1-6] However, the electronic repulsion between the electron-rich functional groups involved, namely the nitrogen lone pair and the alkene/alkyne π-system, as well as the regioselectivity towards the Markovnikov and anti-Markovnikov products, make this reaction challenging. Moreover kinetic and thermodynamic constraints due to the energy difference between the π-system of the C-C multiple bond and σ-(N-H) orbital, the slightly exothermic or even thermo neutral character of the reaction, and the negative entropy of the coupling reaction require an efficient catalyst for obtaining high activity and chemoselectivity under mild conditions. Homogenous catalysts based on metal salts, alkali and earth alkali metal hydroxides, lanthanides and transition metal complexes have been so far reported for both

3

intermolecular and intramolecular hydroamination of alkynes.[1, 4, 5] Gold nanoparticles (AuNPs) stabilized by inorganic oxides (titanium oxide,[7] nitrogen-doped titanium oxide,[8, 9] silica[10]), functionalized silica,[11, 12] surfactants,[13] capping agents,[14] carbon materials[15, 16] and polymers (polyvinylpyrrolidone[17], chitosan[18]) are emerging as promising and recyclable heterogeneous catalyst for this reaction.[7-19]

In this work we report on the performances of the AuNPs catalyst embedded in a nanoporous semicrystalline polymer matrix consisting of syndiotactic polystyrene-*cis*-1,4-polybutadiene multiblock copolymer (sPSB). [20-24] The copolymer with composition rich in styrene (>80 *wt*%) makes the properties of this support similar to those of syndiotactic polystyrene where high affinity and permeability to small organic molecules were demonstrated. Actually aromatic and halogenated molecules are hosted into the nanocavities or nanochannels of the crystalline lattice of the δ and ε crystalline forms, producing co-crystalline phases or intercalates of syndiotactic polystyrene.[25-29] By analogy, the nanopores in sPSB act as a conveyor and concentrator of the reagents towards the gold catalytic sites, making the AuNPs-sPSB catalyst highly efficient in aerobic oxidation of alcohols,[30-32] direct oxidative esterification of alcohols with aliphatic alcohols[31, 32] and selective reduction of nitroarenes to anilines[33].

2. Methods

2.1. General procedures and materials

Air- and moisture-sensitive compounds were manipulated under nitrogen atmosphere using standard Schlenk techniques and MBraun glovebox. The catalytic tests were carried out under inert protective atmosphere (N_2) and dark conditions in the presence of activated molecular

sieves (4A). The sPSB copolymer [20-24] (88 *mol*% of styrene (93 *wt*%)), the AuNPs-sPSB catalyst ([Au] = 2.0 *wt*%)[30-33] and aniline-*N,N-d$_2$*[34] were synthesized and characterized according to the reported procedures. Tetrachloroauric acid trihydrate (≥49.0 *wt*% of Au, Sigma-Aldrich), sodium triethylborohydride (1.0 M in THF; Sigma-Aldrich), phenylacetylene (PA; 98%; Sigma-Aldrich), aniline (AN; 98 %; TCI Chemicals), p-toluidine (99 %; Sigma-Aldrich), 4-chloroaniline (98 %, Sigma-Aldrich), 2,4,6-trimethylaniline (98 %, Sigma-Aldrich), 4-bromoaniline (97 %, Sigma-Aldrich), 1-bromo-4-ethynylbenzene (97 %, Sigma-Aldrich), 4-ethynylanisole (97 %, Sigma-Aldrich), *p*-anisidine (>99 %, Sigma-Aldrich), 4-ethynyltoluene (97 %, Sigma-Aldrich), AuNPs-TiO$_2$ (1 wt%$_{Au}$ on titania support; Strem Chemicals), AuNPs-ZnO (1 wt%$_{Au}$ on zinc oxide; Strem Chemicals), AuNPs-Al$_2$O$_3$ (1 wt%$_{Au}$ on aluminium oxide; Strem Chemicals), AuNPs–CB (1 wt%$_{Au}$ on amorphous carbon black support; Strem Chemicals), gold(III) standard solution for analysis ICP-OES of AuNPs-sPSB (1.000±0.002 g/L of gold in water with 2 wt% of HCl; Carlo Erba Reagenti) and deuterated solvents (Sigma-Aldrich or Eurisotop) were used, unless otherwise stated, as received.

2.2. Hydroamination of phenylacetylene with aniline catalysed by AuNPs-sPSB-t (entry 1 of Table 1)

This general procedure has been applied to all catalytic runs of Table 1 and Table 2 performed with the AuNPs-sPSB-*t* catalyst having the polymer support in the β crystalline form. A 10 mL round bottom flask, equipped with a magnetic stirring bar, was charged with AuNPs-sPSB-*t* (100 mg, [Au] = 0.09 *mol*%), PA (5.08 mmol) and AN (6.09 mmol) corresponding to PA:AN:Au = 500:600:1 molar ratio. The reactor was equilibrated at 100 °C and the reaction was carried out for 7 h under vigorous stirring. The mixture was then cooled at room temperature and DMSO-d$_6$

was added for the precipitation of the catalyst. After centrifugation (4000 rpm) and removal of the solid by filtration, the solution was rapidly analyzed by ^{1}H NMR spectroscopy.

2.3. Kinetic investigation of hydroamination of phenylacetylene with aniline promoted by AuNPs-sPSB-t

The catalytic tests were carried out under pseudo-first-order reaction conditions with respect to AN, AN-d_2 or PA for the determination of the kinetic parameters. A 10 mL round bottom flask, equipped with a magnetic stirring bar, was charged with AuNPs-sPSB-t (100 mg; [Au] = 0.09 $mol\%$), PA, AN, equilibrated at 100 °C and left under stirring for 7 h. The determination of the reaction order for AN or AN-d_2 was conducted using PA (10.51 mmol) and AN (0.66 mol); the determination of reaction order of PA was performed using AN (10.51 mmol) and PA (0.66 mol) corresponding to a (PA+AN):Au molar ratio of 1100:1 and a gold loading of 0.09 $mol\%$. Aliquots were sampled from the reaction mixture under nitrogen; DMSO-d_6 was added for the precipitation of the catalyst that was separated by centrifugation (4000 rpm). The solution was rapidly analysed by ^{1}H NMR spectroscopy. (Table 3).

2.4. Instrumentation and methods

NMR spectra were collected on AVANCE Bruker spectrometers (600, 400 and 300 MHz for ^{1}H). The chemical shifts are referenced to tetramethylsilane, as external reference, using the residual protio signal of the deuterated solvent. ^{1}H NMR chemical shifts of diagnostic signals[35-37] for the reaction products (δ in ppm, DMSO-d_6, 25 °C) are: (*E*)-*N*-1-diphenylethan-1-imine (400 MHz), δ = 7.99 (2H, d, J = 6.4 Hz), 7.52-7.45 (3H, m), 7.36 (2H, t, J

= 7.7 Hz), 7.00 (1H, t, *J* = 7.7 Hz), 6.78 (2H, d, *J* = 7.3 Hz), 2.20 (3H, s); (*E*)-1-(4-bromophenyl)-N-phenylethan-1-imine (400 MHz), δ = 7.92 (2H, d, *J* = 8.6 Hz), 7.68 (2H, d, *J* = 8.5 Hz), 7.36 (2H, t, *J* = 7.8 Hz), 7.08 (1H, t, *J* = 7.4 Hz), 6.79 (2H, d, *J* = 7.2 Hz), 2.18 (3H, s); (*E*)-N-phenyl-1-(p-tolyl)ethan-1-imine (400 MHz), δ = 7.88 (2H, d, *J* = 8.1 Hz), 7.35 (4H, t, *J* = 7.9 Hz), 7.07 (2H, t, *J* = 7.5 Hz), 6.77 (2H, d, *J* = 7.6 Hz), 2.31 (3H, s), 2.17 (3H, s); (*E*)-1-(4-methoxyphenyl)-N-phenylethan-1-imine (400 MHz), δ = 7.95 (2H, d, *J* = 8.8 Hz), 7.34 (2H, t, *J* = 7.8 Hz), 7.04-6.98 (3H, m), 6.76 (2H, d, *J* = 7.3 Hz), 3.82 (3H, s), 2.15 (3H, s); (*E*)-1-phenyl-N-(p-tolyl)ethan-1-imine (δ in ppm) = 8.00-7.94 (2H, m), 7.52-7.44 (3H, m), 7.16 (2H, d, *J* = 7.9 Hz), 6.68 (2H, d, *J* = 8.1 Hz), 2.29 (3H, s), 2.19 (3H, s); (*E*)-N-(4-methoxyphenyl)-1-phenylethan-1-imine (δ = 8.00-7.94 (2H, m), 7.51-7.43 (3H, m), 6.93 (2H, d, *J* = 8.7 Hz), 6.75 (2H, d, *J* = 8.7 Hz), 3.75 (3H, s), 2.21 (3H, s); (*E*)-N-mesityl-1-phenylethan-1-imine (δ in ppm) = 8.02 (2H, d, *J* = 6.6 Hz), 7.53-7.44 (3H, m), 6.86 (2H, s), 2.22 (3H, s), 2.02 (3H, s), 1.90 (6H, s); (*E*)-N-(4-bromophenyl)-1-phenylethan-1-imine (δ in ppm) = 7.98 (2H, m), 7.56-7.45 (4H, m), 7.11 (1H, d, *J* = 8.7 Hz), 6.77 (2H, d, *J* = 8.6 Hz), 2.20 (3H, s); (*E*)-N-(4-chlorophenyl)-1-phenylethan-1-imine (δ in ppm) = 7.98 (2H, m), 7.56-7.44 (4H, m), 7.00 (1H, d, *J* = 8.6 Hz), 6.82 (2H, d, *J* = 8.5 Hz), 2.21 (3H, s); (*Z*)-N-phenyloctan-2-imine (600 MHz) δ = 1.71 (3H, s); (*E*)-N-phenyloctan-2-imine (600 MHz), δ = 2.06 (3H, s).

The gold loading in AuNPs-sPSB was determined by inductively coupled plasma optical emission spectrometry (ICP-OES) with a Optima 7000 DV spectrometer from Perkin-Elmer.[30-33, 38] The AuNPs-sPSB catalyst (50 mg) was acid digested in a Kjeldahl flask by treatment with concentrated sulfuric acid (2.5 mL, 98 *wt*%) at 250 °C for 30 min and then at room temperature with hydrogen peroxide (4.0 mL, 30 *wt*%). The resulting suspension was heated at 250 °C until to produce a clear solution. Aqua regia (1.5 mL) was added at room temperature and

the solution was diluted with an aqueous solution of HCl (10 v%) to a final volume of 10.0 mL. The calibration was performed using seven solutions with variable concentration of gold(III), prepared by progressive dilution of a standard solution (1.000±0.002 g/L in water with 2 wt% of HCl) with water and an aqueous solution of HCl (10 v%).

Wide angle x-ray diffraction (WAXD) patterns have been obtained in reflection mode with an automatic Bruker D8 powder diffractometer using the nickel-filtered Cu K$_\alpha$ radiation.

Conventional transmission electron microscopy (CTEM) was carried out with a Tecnai Spirit transmission electron microscope from FEI, working at acceleration voltage of 120 kV, equipped with a lanthanum hexaboride thermionic electron source and a twin objective lens, and the images were acquired using a Gatan Orius CCD camera. HRTEM was carried out with a Titan transmission electron microscope from FEI, working at acceleration voltage of 300 kV, equipped with an ultra-bright field emission electron source (X-FEG) a super-twin objective lens, and the images were acquired using a Gatan 2k×2k CCD camera. For both CTEM and HRTEM imaging, the specimens were prepared by dispersing and sonicating the AuNPs-sPSB catalyst in isopropanol, followed by the deposition of a small droplet of it onto a grid for TEM imaging (carbon film supported by 300-meshes copper) supplied by TedPella (USA).

XPS measurements were performed at normal angle emission in a Specs setup, using Al Kα monochromated radiation (hν = 1486.7 eV) of an X-ray gun, operating with 300 W (12 kV/25 mA) power. A flood gun with electron acceleration at 1 eV and electron current of 100 mA was used in order to avoid charging effects. The energy of photo ejected electrons is measured using a Phoibos 150 analyser, operating with pass energy of 30 eV. The spectra were fitted using Voigt profiles combined with their primitive functions, for inelastic background. The Gaussian width of all lines and thresholds can be considered constant for each spectrum as they should not differ

considerably from one spectrum to another, being always in the range of 2 eV. The spectra were collected in the energy range corresponding to Au(0) $4f_{7/2}$ Au(0) $4f_{5/2}$ peaks.

2.5. Computational details

Theoretical calculations were carried out by means of the Gaussian 16 program package.[39] All geometry optimizations were carried out using the pure Perdew, Burke and Ernzerhof functional[40] and the Ahlrichs basis set def2-SVP [41] was selected. Since dispersive Au···H–C and Au···π interactions are expected,[42] the Grimme's dispersion correction[43] with Becke-Johnson damping was also included in these optimizations. Analysis of corresponding frequencies were performed to characterize structures of minima ($N_{imag} = 0$) or transition states ($N_{imag} = 1$). All models were built using an Au_{20} cluster obtained from crystallographic coordinates. Initially, Au cluster was optimized using a D_{2h} point group symmetry. Then, all models were optimized on the surface keeping the optimization all Au atoms frozen. Gibbs free energies (ΔG_{298}, in kcal/mol) were used for the discussion on the relative stabilities of the considered structures.

Molecular Electrostatic Potential (MEP) surface of Au_{20} was also calculated at the same level of theory and plotted onto the van der Waal surface (0.001 a.u. isodensity value). The Bader's "Atoms in molecules" theory has been applied by means of the AIMall calculation package.[44]

3. Results

3.1. Synthesis and characterization of the AuNPs-sPSB catalyst

The AuNPs-sPSB catalyst was prepared according to the previously reported procedure.[30-33] The inductively coupled plasma-optical emission spectrometry (ICP-OES) analysis of acidic digested AuNPs-sPSB samples showed that the gold entrapment is quantitative and the final concentration is of 2.0 *wt*%. The powder wide angle x-ray diffraction (WAXD) analysis of *as synthesized* AuNPs-sPSB showed, in the 2θ range from 5° to 30°, signals diagnostic of the co-crystalline δ form of the polymer support containing toluene (Fig. 1a) or THF molecules (Fig. 1b) resulting from the synthetic procedure, clathrated in the voids of the crystalline lattice of the syndiotactic polystyrene phase. The mean size of the AuNPs, calculated with the Scherrer equation applied to the *<111>* reflection of crystalline gold, is of 5.3 nm (Fig. 1b). The conventional (TEM) and high resolution transmission electron microscopy (HRTEM) revealed that the AuNPs are homogeneously embedded in the crystalline polymer matrix (Fig. 2a), with few of them occasionally aggregated (Fig. 2b) or found in irregular cuboctahedral morphology (Fig. 2c). The annealing of the catalyst at 170 °C for 5 h (AuNPs-sPSB-*t*) allows removing the clathrated molecules and converts the polymeric support from δ to β crystalline form (Fig. 1c), the latter showing a compact polymer chain packing [25, 26, 29] with reduced permeability to small organic molecules. During the thermal treatment, a partial coalescence of the naked AuNPs is observed that produces an increase of the average size to 9.0±0.5 nm (Fig. 1c) as well as the formation of both twinned and single AuNPs with spheroidal-like morphology (Fig. 2d-f).

The x-ray photoelectron spectra (XPS) of AuNPs-sPSB revealed the exclusive presence of Au(0) on the catalyst surface showing peaks centred at 84.3 and 87.9 eV consistent with Au(0) $4f_{7/2}$ and $4f_{5/2}$ signals (Fig. 1e).
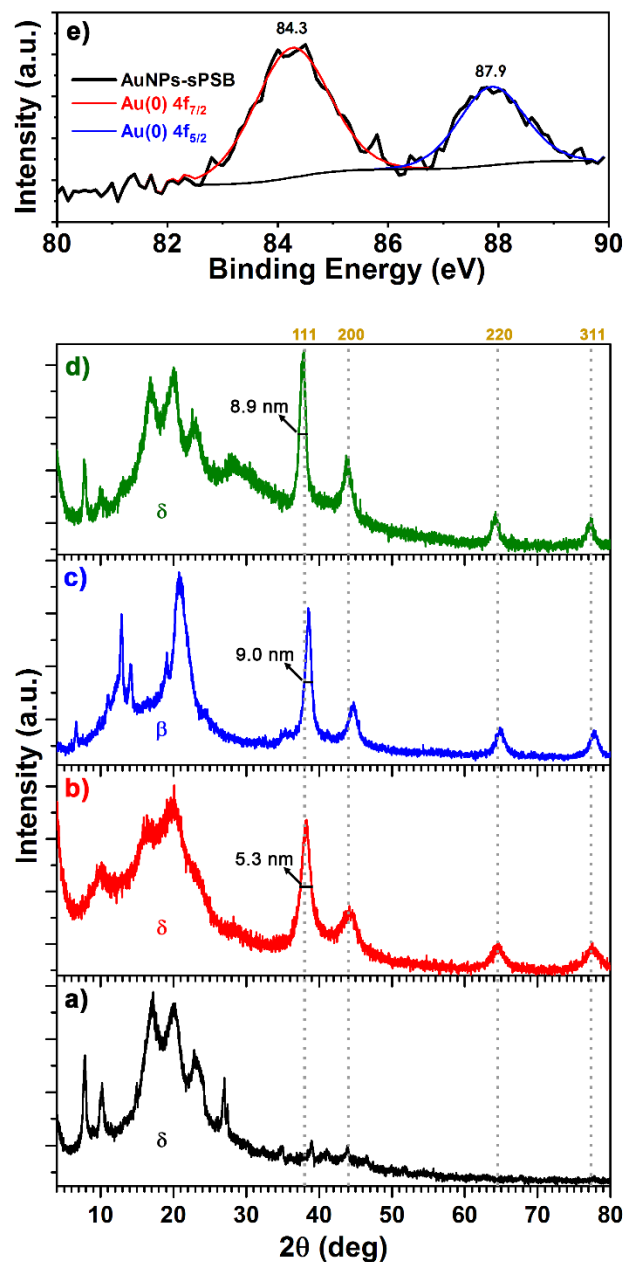
Fig. 1. WAXD patterns of: a) the sPSB polymer support in the δ-crystalline form; b) as synthesized AuNPs-sPSB in the δ-crystalline form; c) AuNPs-sPSB-*t* after annealing at 170 °C for 5 h (observed in the β-crystalline form); d) AuNPs-sPSB-*ct* after a catalytic run carried out under the reaction conditions of entry 1 of Table 1 (observed in the δ-crystalline form). Dotted lines mark the reflections of *fcc* crystalline lattice planes of nanocrystalline gold; e) XPS profile of AuNPs-sPSB with Au(0) $4f_{7/2}$ and $4f_{5/2}$ predicted traces.
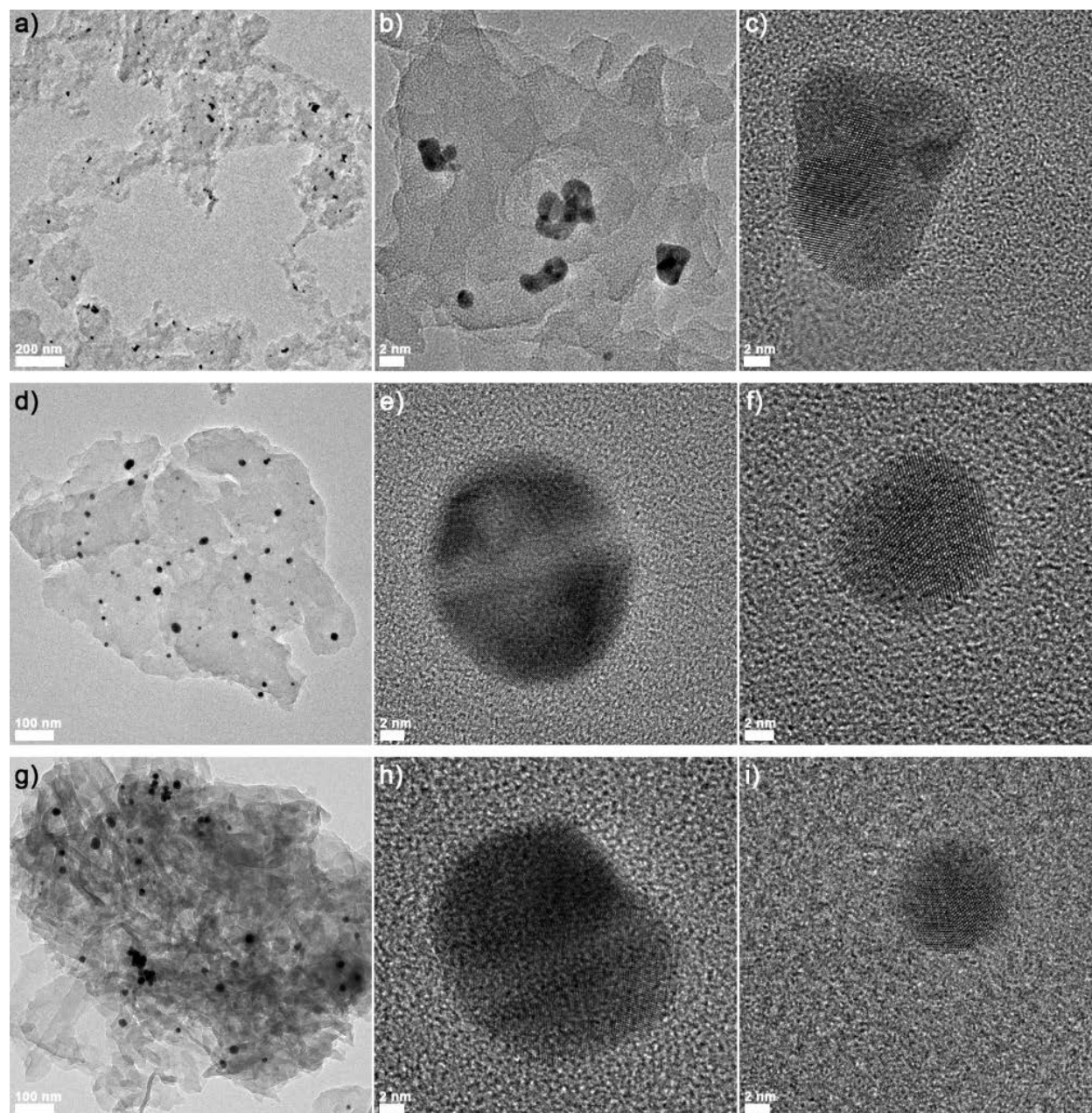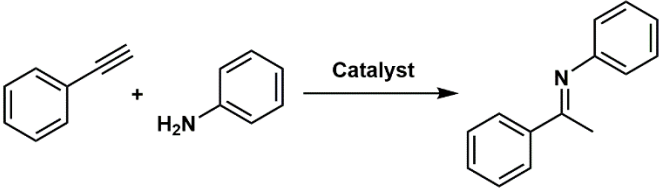
Fig. 2. TEM (panels a, d, g) and HR-TEM (panels b, c, e, f, h and i) images of *as synthesized* AuNPs-sPSB (panels a-c); after thermal treatment at 170 °C for 5h (AuNPs-sPSB-*t*; panels d-f) and after a catalytic run under the reaction conditions of entry 1 of Table 1 (AuNPs-sPSB-*ct*; panels g-i).

3.2. Hydroamination of phenylacetylenes with anilines

The high affinity and permeability of AuNPs-sPSB towards aromatic compounds,[25-29] prompted us to investigate hydroamination of phenylacetylene (PA) with aniline (AN) as a model reaction. Preliminary, the catalytic properties of AuNPs-sPSB-*t* were screened in parallel with those of commercially available gold catalysts, namely AuNPs-TiO$_2$ (1 *wt%*$_{Au}$) AuNPs-Al$_2$O$_3$ (1 *wt%*$_{Au}$), AuNPs-ZnO (1 *wt%*$_{Au}$) and AuNPs-CB (CB = carbon black; 1 *wt%*$_{Au}$).

Anhydrous reagents, inert protective atmosphere and dark conditions were chosen for minimizing the side-effects of water, oxygen and light on the catalyst performances.[4, 8] The AuNPs-sPSB-*t* catalyses the hydroamination of neat PA and AN into the corresponding aromatic *E*-ketimine with conversion values among the highest so far reported for this reaction (90 % in 7 h, entry 1 of Table 1). The head-to-head comparison with the commercial gold catalysts, under the conditions of slight excess of AN (AN:PA molar ratio of 1.2:1) and gold loading of 0.09 *mol*% (AN: PA: Au = 600:500:1 molar ratio) is summarized in Table 1. AuNPs-sPSB-*t* and AuNPs-TiO$_2$ show similar activity producing 90% conversion of PA at 100 °C in 7 h, corresponding to a turnover frequency (TOF) of 64 h^{-1} (entries 1 and 2 of Table 1). The performances of AuNPs-TiO$_2$ were partially unexpected since previous reports highlighted that UV irradiation or acidic co-catalysts are necessary for obtaining high conversion under comparable conditions.[7-9] In all investigated cases the main reaction product is the secondary ketimine derivative, namely the Schiff base with Markovnikov regiochemistry and *E* configuration (Table 1). The PA conversion with AuNPs-Al$_2$O$_3$ (entry 3, Table 1), AuNPs-ZnO (entry 4, Table 1) and AuNPs-CB (entry 5, Table 1) are lower than those obtained with the title catalyst.

13

Table 1. Hydroamination of PA with AN.

Entry [a]	Catalyst	T (°C)	t (h)	Conversion[b,c] (%)	E/Z [c] (molar ratio)	TON [c,d]	TOF [c,e] (h^{-1})
1	AuNPs-sPSB-*t*	100	7	90	>99:1	450	64
2	AuNPs-TiO$_2$	100	7	90	>99:1	450	64
3	AuNPs-Al$_2$O$_3$	100	7	65	>99:1	325	46
4	AuNPs-ZnO	100	7	28	>99:1	140	20
5	AuNPs-CB	100	7	81	>99:1	405	58
6	AuNPs-sPSB-*t*	60	1	5	>99:1	25	25
7	AuNPs-sPSB-*t*	80	1	23	>99:1	115	115
8	AuNPs-sPSB-*t*	100	1	45	>99:1	225	225
9	AuNPs-sPSB-*t*	120	1	64	>99:1	320	320
10[f]	AuNPs-sPSB-*t*	60	1	27	>99:1	135	135
11[f]	AuNPs-sPSB-*t*	80	1	43	>99:1	215	215
12[f]	AuNPs-sPSB-*t*	100	1	63	>99:1	315	315
13[f]	AuNPs-sPSB-*t*	120	1	83	>99:1	415	415
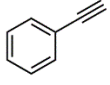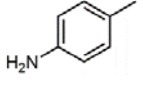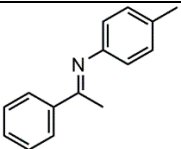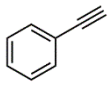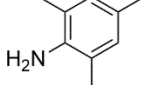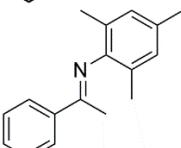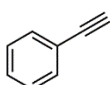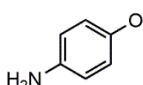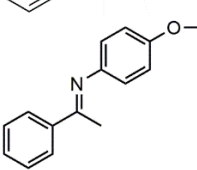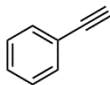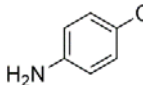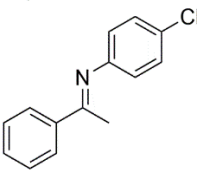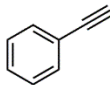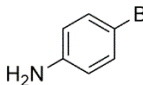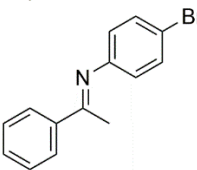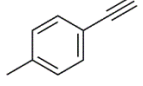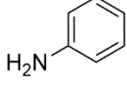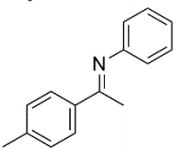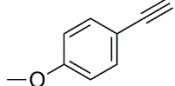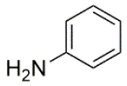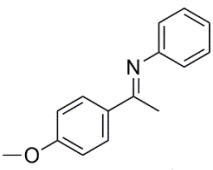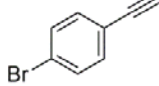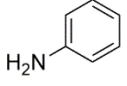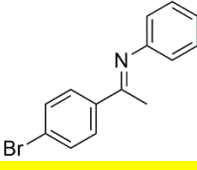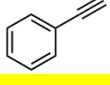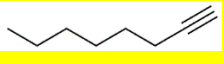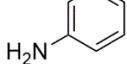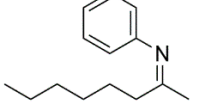
[a] Reaction conditions: PA (5.08 mmol); AN (6.09 mmol); AuNPs-sPSB-t (Au loading of 0.09 *mol*%); PA:AN:Au = 500:600:1 molar ratio. [b] Conversion of PA. [c] Determined by ^{1}H-NMR analysis of the reaction mixture (DMSO-d_6, 25 °C). [d] Turnover number (mol$_{product}$/mol$_{Au}$). [e] Overall turnover frequency (TON/reaction time). [f] Runs carried out with AN-d_2.

The reaction temperature strongly affects the reaction rate. The screening of the catalytic activity was performed at low conversion of PA and AN, using a reaction time of 1h in the temperature range 60-120°C (entries 6-9 of Table 1); as expected the conversion increases with temperature leaving totally unaffected the selectivity of the reaction.

To gain information on the reaction mechanism (*vide infra*) the hydroamination reaction was carried out with aniline-*N,N-d$_2$* (AN-*d$_2$*) under the same experimental conditions (entries 10-13 of Table 1). The activity of AuNPs-sPSB-*t* dramatically drops at 60°C and linearly increases up to 120°C; surprisingly the reactivity of AN-*d$_2$* exceeds that of AN in the range of temperature explored (compare entries 10-13 with 6-9 of Table 1). The TOF values calculated at low conversion reached in this case the excellent value of 225 and 320 h^{-1} in 1h at 100°C and 120 °C that are among the highest so far reported for heterogeneous gold catalysts.[7-19]

Table 2. Scope of the hydroamination reaction of PAs with ANs promoted by AuNPs-sPSB-*t*.

Entry[a]	Alkyne	Aniline	Product[b]	Conv.[b,c] (%)	E/Z[b]	TON[b,d]	TOF[b,e] (h⁻¹)
1				78	>99:1	392	56
2				91	>99:1	458	65
3				94	>99:1	473	68
4				96	>99:1	483	69
5				99	>99:1	498	71
6				65	>99:1	327	47
7				89	>99:1	444	64
8				80	>99:1	402	57
9[f]				<1	n.d.	n.d	n.d
10[f]				48	27:73	96	4

16

3.3. Scope of the reaction

The scope of the hydroamination reaction of alkynes catalysed by AuNPs-sPSB-*t* was explored investigating the coupling of PAs and ANs carrying electron-withdrawing (EWG) and electron-donating (EDG) groups onto the aromatic rings; the reaction conditions of entry 1 of Table 1 were adopted for all the catalytic tests (100 °C; molar ratio PA:AN:Au = 500:600:1; gold loading of 0.09 *mol%*). The main results are reported in Table 2. In the case of PAs and ANs, the yields are excellent and the selectivity high in favour of the Markovnikov product showing the thermodynamic favoured *E* configuration [ΔE_{ZPE} (*E*-isomer)= –2.4 kcal/mol]. The introduction of EWGs onto the aromatic groups of AN produces a limited effect, being all activity values high, with the TOF values ranging from 56 h^{-1} to 61 h^{-1}. The effect of the EWG groups onto the PAs seems to be more pronounced, determining an increase of the TOF values from 47 h^{-1}, for the methyl *p*-substituent, to 57 h^{-1} and 64 h^{-1} for the bromo- and methoxy- *p*-substituted analogues; however a mesomeric effect can also be invoked in the latter case (entry 3, Table 2).

Compared to PAs and ANs, the preliminary screening of the performances of aliphatic amines and alkynes, typically used in gold catalysed synthesis of imines,[1, 4, 5, 45] showed that these compounds are less reactive than the aromatic analogues (see entries 9 and 10 of Table 2). The coupling of PA with 1-hexylamine is unproductive also when the reaction is carried out at high catalyst loading (0.22 *mol%*$_{Au}$) and prolonged reaction time (24 h) (entry 9, Table 2) whereas the coupling of 1-octyne with AN (entry 10, Table 2) showed low TOF and scarce selectivity under the same conditions. These results are comparable to those observed in alcohols oxidation catalysed by AuNPs-sPSB [25, 26, 30-32] where aliphatic alcohols were found less reactive than aromatic alcohols. More interestingly, a kinetic investigation highlighted that the reaction is of first order for e.g. benzyl or cinnamyl alcohol and of zero order for ethanol and 1-butanol. It was

proposed that a fast diffusion of the aromatic reagents occurs through the porous polymeric support whereas a diffusion controlled kinetics is active in the case of aliphatic alcohols that penetrate the polymeric support likely through the amorphous phase."

3.4. Catalyst recycling

The reusability of AuNPs-sPSB-*t* was checked in repeated catalytic hydroamination of PA with AN at 100 °C under the reaction conditions of entry 8 of Table 1 (Table S1; Fig. 3). In the first catalytic run AuNPs-sPSB-*t* confirmed the excellent TOF of 226 h^{-1}; this value drops to 176 h^{-1} in the second run, remaining constant in the following runs (entries S2-4 of Table S1; Fig. 3). It was previously observed that the repeated intramolecular hydroamination catalysed by AuNPs-TiO$_2$ produces a gold leaching of about 10%. [46] At the first sight the same seems occurring in this study, favoured by the swelling of not crosslinked polymer matrix in aromatic solvents/reactants; however we found that this is not the case since both the gold concentration in the support and the catalytic activity are constant in the consecutive runs. To explain this effect we propose a partial reconstruction of the surface of the AuNPs promoted by AN; a rearrangement of the gold atoms on the nanoparticle surface has been observed at the boundaries of grains in similar multigeminate defective AuNPs.[47] Noteworthy a modification of the crystalline phase of the polymer support, from the not permeable β crystalline form in AuNPs-sPSB-*t,* to the porous δ form was observed just during the first catalytic run (Fig. 1c,d).

19
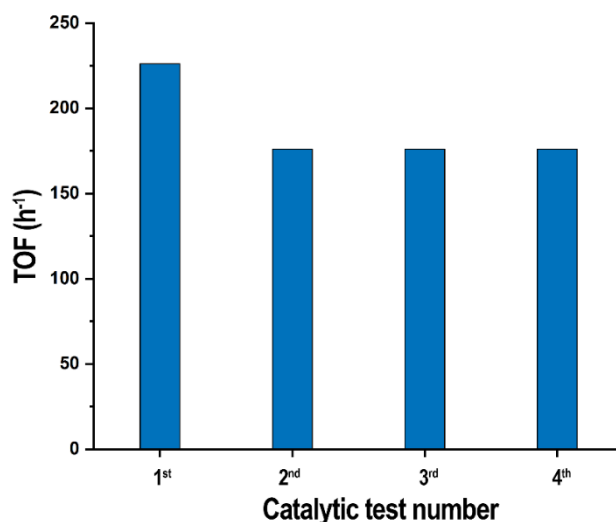
Fig. 3. Catalyst recycling tests in hydroamination of PA with AN at 100°C (reaction conditions in Table S1)

3.5. Mechanistic investigations

Aiming to gain insight into the hydroamination mechanism catalysed by AuNPs-sPSB-*t*, the kinetic order of the reagents under solventless conditions was investigated. Table 3 reports the kinetic parameters for the reaction of PA with AN, or deuterated aniline AN-d_2, under pseudo-first-order reaction conditions using gold loading of 0.09 *mol%*. The conversion plots *vs* time in the temperature range 60°C–100°C are best fitted with pseudo-first order kinetics with regard to both AN (Fig. S1) and PA (Fig. S3), providing specific kinetic constants in the range of 0.825 – 7.94 10^{-4} s^{-1} (Table 3). The corresponding Eyring plot gives a free energy of activation $\Delta G^{\ddagger}$ of 26.6±0.7 kcal mol^{-1} with $\Delta H^{\ddagger}$ of 13.4±1.8 kcal mol^{-1} and $\Delta S^{\ddagger}$ *of* –0.04±0.04 kcal mol^{-1} K^{-1} respectively (Table 3 and Fig. S1). Hence, the enthalpic contribution is higher than the entropic one, that is negative as expected for a coupling reaction. Interestingly AN-d_2 behaves differently than AN in the coupling with PA. The conversion plot is best fitted with a second order kinetics with respect to AN-d_2 and first order with respect to PA (see Table 3 and Fig. S2). The specific

20

kinetic constants are in the range of 0.455 – 6.94 x 10^{-3} L mol^{-1} s^{-1}, thus higher in value than those observed with AN. In agreement with these outcomes, the coupling with PA with AN-d_2 proceeds faster at short reaction time, when the concentration of AN-d_2 is high and is slower at prolonged reaction time, as expected for a reaction profile with kinetic of second order (see Fig. S3, S1a and S2a). The corresponding Eyring plot gives a $\varDelta G^{\ddagger}$ of 25.1±0.5 kcal mol^{-1} with $\varDelta H^{\ddagger}$ and $\varDelta S^{\ddagger}$ values respectively of 16.1±0.9 kcal mol^{-1} and −0.03±0.03 kcal mol^{-1} K^{-1} (Table 3; Fig. S2c). The kinetic isotopic effect (KIE) of this reaction (k_H/k_D = 0.18 at 60°C; = 0.09 at 80°C; = 0.11 at 100°C) is negligible under the experimental conditions explored.

Table 3. Kinetic parameters for hydroamination of PA with AN or AN-d_2.

Entry[a]	Aniline	T	k	$\Delta G^{\ddagger}$	$\Delta H^{\ddagger}$	$\Delta S^{\ddagger}$
		(°C)		(kcal/mol)	(kcal/mol)	(kcal/molK)
1		60	$0.825 \cdot 10^{-4} \pm 6.6 \cdot 10^{-7}\ s^{-1}$			
2	AN	80	$1.91 \cdot 10^{-4} \pm 5.5 \cdot 10^{-6}\ s^{-1}$	26.6±0.7	13.4±1.8	-0.04±0.04
3		90	$4.59 \cdot 10^{-4} \pm 1.6 \cdot 10^{-5}\ s^{-1}$			
4		100	$7.94 \cdot 10^{-4} \pm 3.2 \cdot 10^{-5}\ s^{-1}$			
5		60	$0.455 \cdot 10^{-3} \pm 8.9 \cdot 10^{-6}\ mol^{-1}\ s^{-1}$			
6	AN-d_2	80	$2.180 \cdot 10^{-3} \pm 5.4 \cdot 10^{-6}\ mol^{-1}\ s^{-1}$	25.1±0.5	16.1±0.9	-0.03±0.03
7		100	$6.94 \cdot 10^{-3} \pm 1.2 \cdot 10^{-5}\ mol^{-1}\ s^{-1}$			

[a] Reaction conditions: PA (10.51 mmol), AN or AN-d_2 (0.66 mmol), AuNPs-sPSB-t (100 mg, [Au] = 0.09 *mol*%; PA:AN:Au =1035:65:1 molar ratio (the methodology for the evaluation of the kinetic constants and the reaction order is reported in the SI).

3.6. DFT modelling of hydroamination of PA with AN over AuNPs

In order to shed light on the reaction mechanism of hydroamination of alkynes catalysed by AuNPs-sPSB, DFT calculations were carried out at 298 K using the Au$_{20}$ cluster as model mimicking the corners, edges and planes located on the surface of the nanoparticle. Firstly, the analysis of the molecular electrostatic potential (MEP) was applied to understand the most favourable adsorption sites on the surface of the Au$_{20}$ cluster. The calculated values reveal some positive regions (+14 kcal/mol) that allow PA coordination along with negative regions (−6.0 kcal/mol) as feasible adsorption sites for AN (Fig. 4). The adsorption of AN onto the surface is even better than PA ($\Delta\Delta E_{ads}$ = −1.0 kcal/mol). MEP surface analysis suggests that AN coordination strongly reduces the nucleophilic capability of this reagent (V = +30.7 kcal/mol) that should thus require pre-activation to afford the hydroamination reaction. A photocatalytic

22

activation in AuNPs-TiO$_2$ by the TiO$_2$ support was proposed to overcome this drawback; a radical cations is first generated, followed by electrophilic attack to PA.[9] The results herein provided seem to rule out this hypothesis because an organic polymer support provides comparable if not better catalytic performances than the photoactive TiO$_2$. Alternatively N-H σ-bond activation[16] (see Scheme 1a and Fig. S6) or deprotonation with Brønsted bases were proposed for reducing the steric hindrance at the nitrogen atom and to promote the electrophilic attack to coordinated PA. The calculated energetic barrier for this reaction step on Au$_{20}$ is too large (ΔG_{298} = 50.1 kcal/mol) when compared to the experimental values obtained in the kinetic investigation.
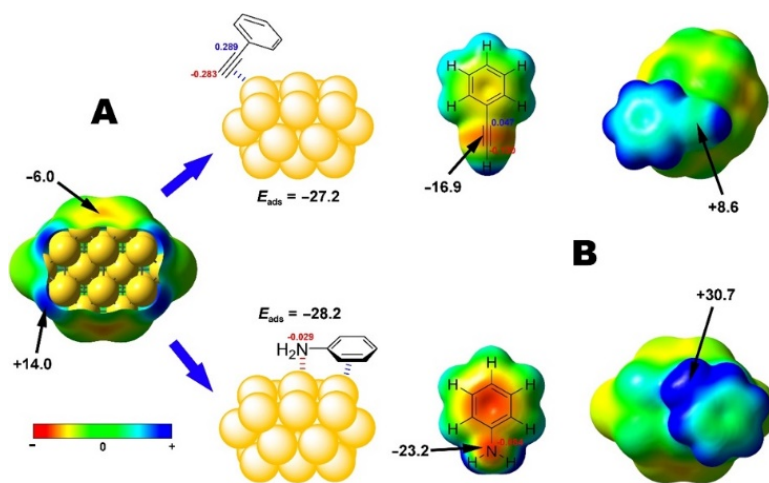
Fig. 4. MEP plotted on the van der Waals surface and Mulliken charges of representative carbons (energies are given in kcal/mol).
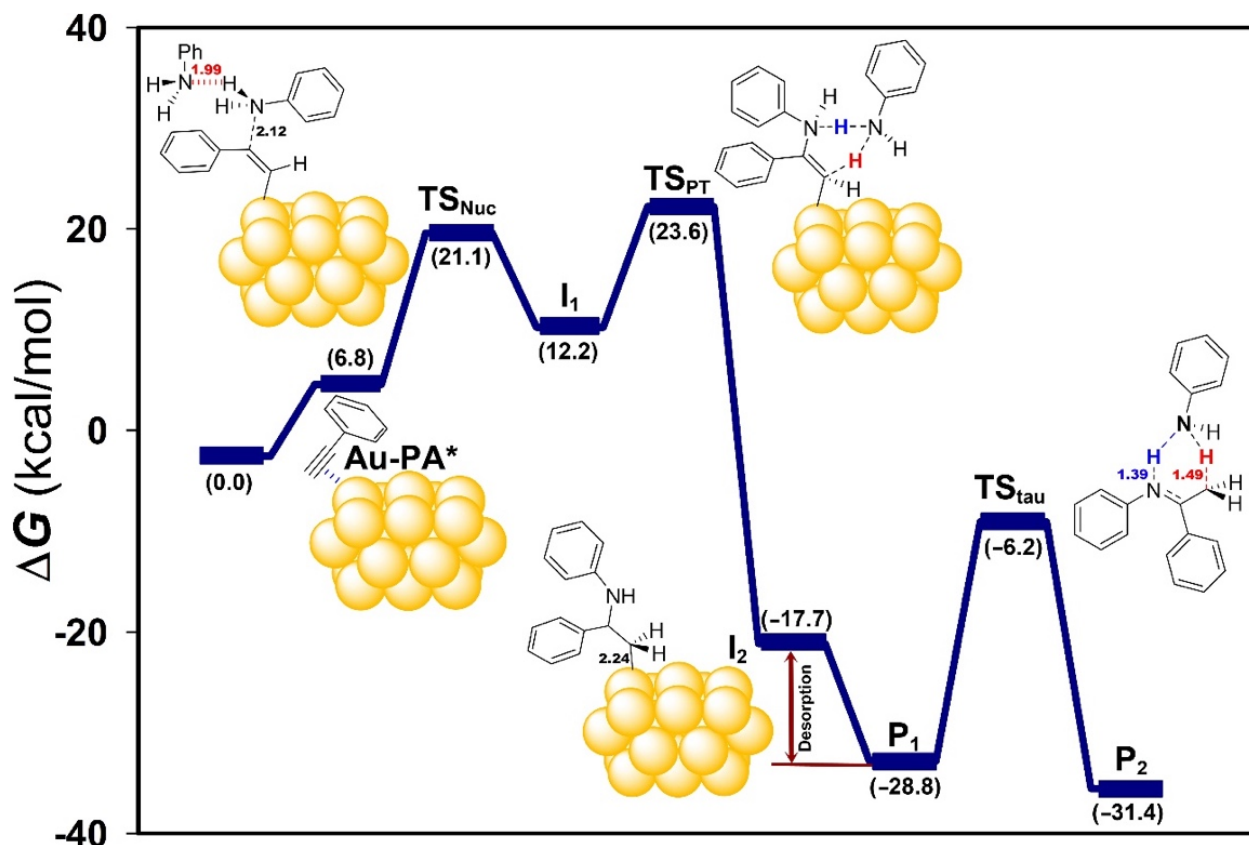
Fig. 5. Gibbs energy profile for the hydroamination of PA with AN catalysed by Au_{20} cluster at 298 K. Schematic structures for the representative species are shown (distances are in Å).

A simple inspection of Mulliken's charge or even the corresponding MEP surface of PA (Fig. 5b, $V_{c≡c} = -16.9$ kcal/mol) reveal a negative electron density that makes difficult the attack to AN coordinated on gold because of an electrostatic repulsion. The AuNPs surface seems to mimic the acidic conditions of Brønsted acids or activation by cationic transition metal complexes that modify the electron density of PA (Fig. 5b, $V_{c≡c} = +8.6$ kcal/mol). The activation Gibbs energy calculated for the nucleophilic attack of AN to coordinated PA on Au_{20} is of 30.6 kcal/mol ($\Delta G^{\ddagger}_{Nuc}$) that is higher than the experimental value ($\Delta G^{\ddagger}_{exp} = 26.6$ kcal/mol) found in the kinetic investigation (see Table 3 and Fig. 5). To improve the quality of the reaction modelling we considered that the possibility of hydrogen bonding interaction with a second AN molecule (Fig.

5). The same could occur in the following reaction steps where the proton transfer can be assisted by a AN molecule as a proton shuttle; these intermediate species were proposed in the hydroamination reaction with hydrazine.[48] The reaction pathway modelled on the basis of this assumption gives the optimized structure of the transition state corresponding to the nucleophilic attack of AN to PA (TS$_{Nuc}$) at C$_\alpha$ [$\delta^+$$_{(C\alpha)}$ = 0.289], affording the Markovnikov-type addition (I$_1$) shown in Fig. 5. This hydrogen bond-assisted TS$_{Nuc}$ presents a N$\cdots$C distance of 2.12 Å (approaching angle of 111º) and leads to a $\Delta G^\ddagger_{Nuc}$ of 21.1 kcal/mol. To characterize this hydrogen bonding interaction, the Bader`s theory Atoms in Molecules was also successfully applied and the following values $R_{N\cdots H2N}$ = 1.99 Å and ρ = 0.0433 a.u. were calculated (Fig. S7).

Upon formation of the C-N bond, a proton transfer may proceed through a stepwise or a concerted mechanism. The stepwise mechanism presumably involves a transition state (TS$_{PT1}$), intermediate I$_{PT}$ and another TS$_{PT1'}$. These consecutive steps should finally afford the enamine-bound intermediate I$_2$ (R_{C-Au} = 2.24 Å) which presents η^1-coordinated enamine. Firstly, we evaluated the role of AN to draw a proton from the amine moiety (I$_1$) to produce an anilinium cation [Ph(NH$_3$)$^+$]. The removal of a N-H proton affording the I$_{PT}$ intermediate, stabilized by the anilinium counterion, is not favoured in this case. In fact, this situation drives to a concerted mechanism with a large barrier ($\Delta G^\ddagger_{PT}$ of 23.6 kcal/mol) in which another proton is simultaneously transferred to terminal carbon (TS$_{PT}$). For this reason, we explored a concerted mechanism in which two AN molecules are involved in. In this case, a proton transfer to AN (I) and the fleeting anilinium cation released another proton to a second AN molecule (II) which subsequently transferred a proton to C$_\alpha$ carbon of the coordinated alkyne to form the aforementioned intermediate I$_2$ (see Fig. S8). Despite this feasibility, TS$_{PT1}$ was not found in the potential energy surface since TS$_{PT1}$ and I$_{PT}$ displayed an energy difference (ΔE) between them

less than 2 kcal/mol (Fig. S9). Contrarily, the Gibbs energy difference between I_{PT} and $TS_{PT1'}$ was calculated in 7.0 kcal/mol. Similar to previous studies, the thermodynamic driving force of this reaction is the formation of imine P_2, 31.4 kcal/mol more stable than reactants. In this context, a new insight arises from Au_{20} cluster as model for gold nanoparticles. The coordinated enamine I_2 is more stable than imine one (I_3, $\Delta\Delta G = -1.4$ kcal/mol), and therefore, is the thermodynamic product of this reaction. However, the desorption from the surface is strongly favoured ($\Delta\Delta G_{des} = -11.1$ kcal/mol). When enamine tautomer P_1 (pro-Z configuration) is desorbed, it suffers a subsequent tautomerization step (calculated barrier, $\Delta G^{\ddagger}_{tau} = -6.2$ kcal/mol) to finally afford the (Z)-imine product P_2 ($\Delta\Delta G = -2.6$ kcal/mol). The proton transfer of this tautomerization is again mediated by aniline where the TS_{tau} shows both N-H bond breaking ($R_{N-H} = 1.39$ Å) and C-H bond formation ($R_{C-H} = 1.49$ Å). This pro Z-configured TS_{tau} indicates that Z-isomer is the kinetically favoured ($\Delta G^{\ddagger}_{tau} = 1.5$ kcal/mol for E-configuration). Once Z-imine P_2 is formed, a thermal isomerization afforded the thermodynamically E-imine P_2' product ($\Delta G_{P2'} = -33.9$ kcal/mol).[49]

4. Discussion

Mechanistic studies on the hydroamination reaction of PAs with ANs catalysed by gold are few and mainly focused on homogeneous Au(I) catalysts.[5, 8, 9, 16, 50] Two main routes, depicted in Scheme 1, can be conceived depending on which reactant is activated onto gold surface, namely AN or PA.[1] In heterogeneous catalysis by Au(0), the proposed reaction mechanism, supported by DFT calculation,[16] proceeds through: *i*) coordination/activation of the N-H σ-bond and coordination of the π system of PA onto the gold surface; *ii*) insertion of the PA into N-Au bond; *iii*) reductive elimination of the enamine from the surface of the AuNPs followed by

tautomeric isomerization to ketimine (Scheme 1a). The alternative alkyne insertion into Au-H bond could produce the corresponding aldimine derivative (Fig. S6, reaction pathway c'-d').[1, 16]

The acid catalysed reaction pathway, typical of homogeneous Au(I) catalysts, involves: *i*) activation/coordination of the C≡C triple bond to electrophilic species (Au(0) or Au(I)); *ii*) nucleophilic attack of the amine to π-system of alkyne; *iii*) proton transfer from the anilinium cation to the alkenyl-gold, generating the enamine intermediate; iv) tautomeric rearrangement of the enamine into the corresponding Markovnikov ketimine (see Scheme 1b).

The kinetic investigation herein reported supports the mechanistic pathway involving the preliminary activation of the alkyne onto gold surface of AuNPs-sPSB-t (Scheme 1b) that enhances the reactivity of the PAs towards nucleophiles in agreement with the well-known "*alkynophilic*" behaviour of the gold.[45] The presence of EWGs on the aromatic rings of PA indeed increases the electrostatic polarization of the triple C≡C bond favouring the nucleophilic attack of the amine at the $C\alpha$ (see Table 2 and Table 1). The DFT calculation highlighted that the energetic barrier of this reaction step decreases as the number of AN molecules increases in the transition step, where the formation of AN aggregates stabilized by hydrogen bonding have been proposed. The nucleophilicity of AN involved in the N-C bond forming reaction is thus increased in this way and yields lower energetic barrier (< 21.1 kcal mol^{-1}). In conclusion, this cannot be considered the rate determining step in hydroamination reaction. The following reaction step consists of a 1,3-hydrogen shift from the anilinium cation to the C_β of the enamine intermediate (vinyl-Au) bound to the gold surface. The transition state TS_{PT} of Fig. 5 decreases in energy to 23.6 kcal mol^{-1} when one additional AN molecule is involved in the proton shuttling; this value is now comparable to the experimental activation energy found in the kinetic

experiments and supports the pseudo-first order kinetics found for AN in the rate determining step. If this is the case the interpretation of the kinetic order for AN-d_2 is not straightforward. The reaction rates are always higher in the explored range of temperature (60-120°C; Table 3) and second order kinetics has been found for this reagent. Noteworthy a non-negligible inverse KIE was found that is partially surprising in view of the reaction mechanism previously proposed in the literature.[16] This feature of the reaction mechanism cannot be explained in a simple way in view of the multistep reaction pathway and deserves a more accurate investigation of the energy values of the reaction intermediates.

The ^{1}H NMR analysis of the aromatic ketimine resulting from the reaction of PA with AN-d_2 shows an unexpected distribution of deuterated compounds at the methyl group of the arylketimine, namely -CH_3, -CDH_2, -CD_2H and -CD_3, in the 4:22:33:41 molar ratio (Fig. S5). This outcome could result from isotopic scrambling between AN-d_2 and PA, in the pre-activation step, or in the ketimine-enamine tautomerism assisted by AN-d_2. The first hypothesis supports the complex reaction pathway opened by AN-d_2 in which likely more than one AN molecule could be involved in the transition state for the proton shuttling. The ketimine-enamine tautomerism assisted by AN-d_2 was investigated by ^{1}H NMR analysis (Fig. S6) in the absence of the gold catalyst at 80°C. The reaction of ketimine (E)-N,1-diphenylethan-1-imine with AN-d_2 yields the expected isotopic scrambling via an equilibrium reaction among the species in the absence of gold, as predicted from the DFT calculation.
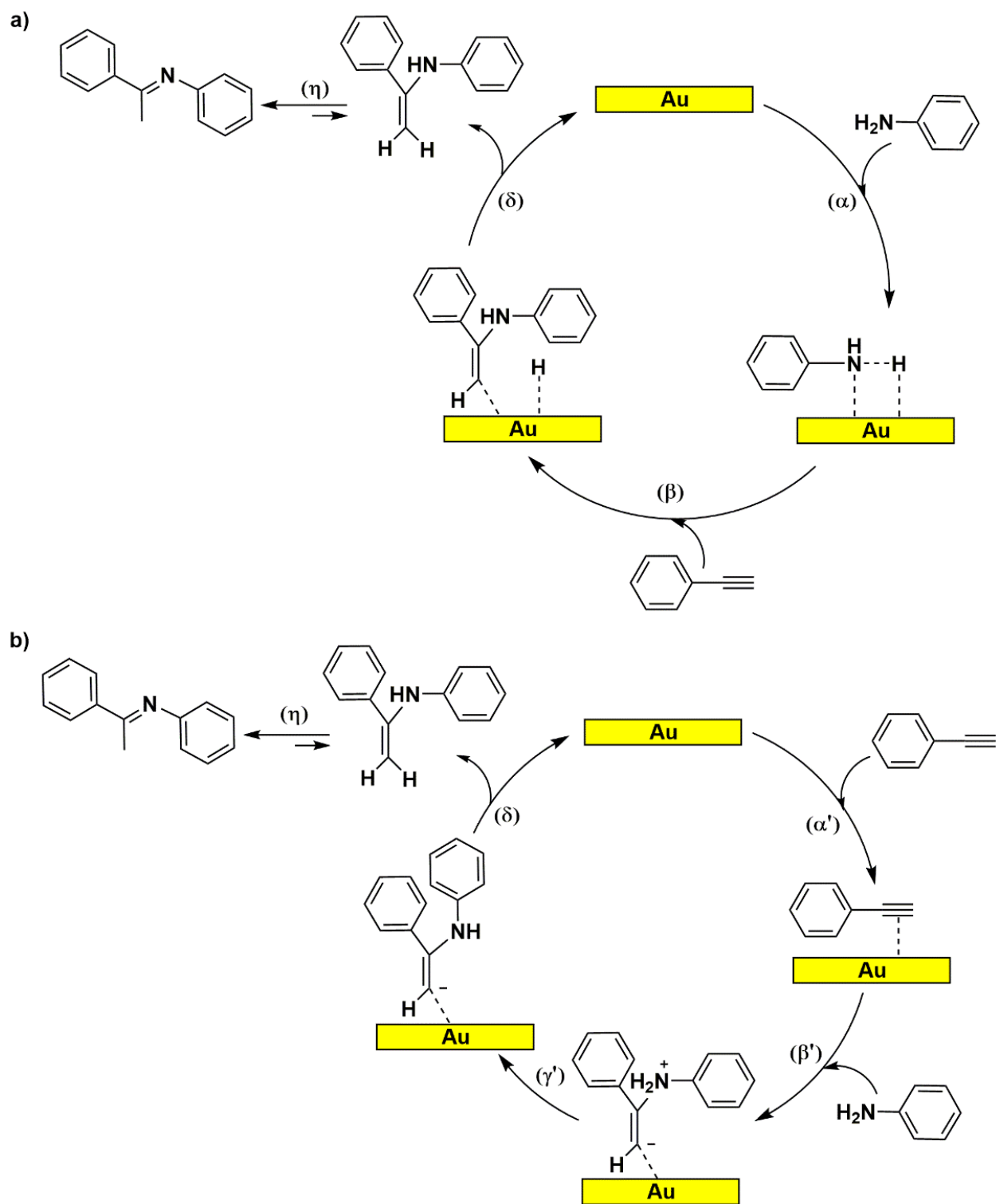
Scheme 1. Possible reaction pathways for gold catalysed hydroamination of PA with AN via amine (a) or alkyne (b) pre-activation.

29

5. Conclusions

In this paper we have shown that AuNPs-sPSB-*t* is a very efficient catalyst in intermolecular hydroamination of ANs with PAs. The naked AuNPs are stabilized by the aromatic rings of the polymer support via weak not bonding interaction; compared to the conventional metal oxides inorganic support we can rule out in this case any synergistic effect between the catalytic properties of the AuNPs and the support. The highest TOF value in hydroamination reaction of PA and AN were reached without introducing acidic activator or photosensitive support. Moreover the nanoporosity of the crystalline polymer phase allows fast diffusion of the reagents to the catalytic sites located at the surface of the nanoparticles as demonstrated by the first order kinetics of AN and PA. The selective formation of the corresponding *N*-arylketimine, found in the thermodynamic favoured *E* configuration, has been accomplished with high stereo- and regio-control under mild conditions, highlighting the greenness of this process in solventless conditions. AuNPs-sPSB-*t* was found robust and stable at 100°C; it was successfully recycled for four times showing only a small drop of the catalytic activity after the first catalytic run as a result of crystallinity of the polymer phase that acts as physical crosslinks. The slight decrease in activity observed only in the second run was attributed to a reconstruction of the defective nanoparticle surface in the presence of the reactants. The excellent TOFs of 225 and 320 h^{-1} obtained at 100°C and 120 °C are the highest so far reported for heterogeneous gold catalysts.

A new reaction pathway for the hydroamination catalysed by AuNPs-sPSB has been proposed on the basis of kinetic investigations supported by the DFT calculations. The rate determining step in this reaction is generally identified in the nucleophilic attack of the AN to alkynes; actually deprotonation of ANs with a base, or the N-H σ-bond activation onto the AuNPs surface are necessary to reduce the electron density at the nitrogen atom and increase its nucleophilicity. The

calculated energetic barrier for the latter reactions, however, is higher than the experimental value determined in the kinetic study of this work. DFT modelling of the hydroamination reaction strongly suggested the formation of AN aggregates, stabilized by hydrogen bonding interactions, that increases nucleophilicity of the AN nitrogen atom, leading to a lower energetic barrier in the reaction with activated/coordinated PA onto the gold surface. The next reaction step is the intramolecular 1,3-hydrogen shift from the nitrogen atom of vinyl-anilinium cation to the Cα of the coordinated enamine intermediate. If this reaction is cooperatively assisted by one AN molecule, the transition state TS_{PT} decreases in energy reaching the value of 23.6 kcal/mol that is in good agreement with the activation energy found in the kinetic study. Our proposal is that this elementary reaction is the rate determining step, in agreement with the pseudo-first order kinetics determined for AN. The absence of KIE rules out that the N-H σ-bond activation could be the key-step of the reaction. In the presence of AN-d_2 a more complex reaction pathway could be anticipated on the basis of the second order kinetics observed for this reagent and the resulting isotopic distribution in the deuterated ketimine product.

Author Contributions

The manuscript was written through contributions of all authors. All authors have given approval to the final version of the manuscript.

Declaration of Competing Interest

The Authors declare no competing financial or non-financial interest.

Acknowledgements

Appendix A. Supplementary material

Supplementary data to this article can be found online.

References

[1] L. Huang, M. Arndt, K. Gooßen, H. Heydt, L.J. Gooßen, Late Transition Metal-Catalyzed Hydroamination and Hydroamidation, Chem. Rev., 115 (2015) 2596-2697.

[2] R. Mancuso, R. Dalpozzo, Recent Progress in the Transition Metal Catalyzed Synthesis of Indoles, Catalysts, 8 (2018) 458.

[3] V.I. Isaeva, L.M. Kustov, Catalytic Hydroamination of Unsaturated Hydrocarbons, Top. Catal., 59 (2016) 1196-1206.

[4] T.E. Müller, K.C. Hultzsch, M. Yus, F. Foubelo, M. Tada, Hydroamination: Direct Addition of Amines to Alkenes and Alkynes, Chem. Rev., 108 (2008) 3795-3892.

[5] R. Severin, S. Doye, The catalytic hydroamination of alkynes, Chem. Soc. Rev., 36 (2007) 1407-1420.

[6] M. Patel, R.K. Saunthwal, A.K. Verma, Base-Mediated Hydroamination of Alkynes, Acc. Chem. Res., 50 (2017) 240-254.

[7] S. Liang, L. Hammond, B. Xu, G.B. Hammond, Commercial Supported Gold Nanoparticles Catalyzed Alkyne Hydroamination and Indole Synthesis, Adv. Synth. Catal., 358 (2016) 3313-3318.

[8] J. Zhao, Z. Zheng, S. Bottle, C. Chen, Y. Huang, S. Sarina, A. Chou, H. Zhu, Factors influencing the photocatalytic hydroamination of alkynes with anilines catalyzed by supported gold nanoparticles under visible light irradiation, RSC Adv., 6 (2016) 31717-31725.

[9] J. Zhao, Z. Zheng, S. Bottle, A. Chou, S. Sarina, H. Zhu, Highly efficient and selective photocatalytic hydroamination of alkynes by supported gold nanoparticles using visible light at ambient temperature, Chem. Commun., 49 (2013) 2676-2678.

[10] V.A. Solovyeva, K.B. Vu, Z. Merican, R. Sougrat, V.O. Rodionov, One-Pot Synthesis of Au@SiO2 Catalysts: A Click Chemistry Approach, ACS Combinatorial Science, 16 (2014) 513-517.

[11] F.-X. Zhu, W. Wang, H.-X. Li, Water-Medium and Solvent-Free Organic Reactions over a Bifunctional Catalyst with Au Nanoparticles Covalently Bonded to HS/SO3H Functionalized Periodic Mesoporous Organosilica, J. Am. Chem. Soc., 133 (2011) 11632-11640.

[12] C. Parise, B. Ballarin, D. Barreca, M.C. Cassani, P. Dambruoso, D. Nanni, I. Ragazzini, E. Boanini, Gold nanoparticles supported on functionalized silica as catalysts for alkyne hydroamination: A chemico-physical insight, Appl. Surf. Sci., (2019).

[13] L.-C. Lee, Y. Zhao, Room Temperature Hydroamination of Alkynes Catalyzed by Gold Clusters in Interfacially Cross-Linked Reverse Micelles, ACS Catal., 4 (2014) 688-691.

[14] T. Nagata, Y. Adachi, Y. Obora, Thiolate-Protected Au25(SC2H4Ph)18 Nanoclusters as a Catalyst for Intermolecular Hydroamination of Terminal Alkynes, Synlett, 29 (2018) 2655-2659.

[15] A. Seral-Ascaso, A. Luquin, M.J. Lázaro, G.F. de la Fuente, M. Laguna, E. Muñoz, Synthesis and application of gold-carbon hybrids as catalysts for the hydroamination of alkynes, Appl. Catal., A, 456 (2013) 88-95.

[16] M. Sengupta, A. Bag, S. Das, A. Shukla, L.N.S. Konathala, C.A. Naidu, A. Bordoloi, Reaction and Mechanistic Studies of Heterogeneous Hydroamination over Support-Stabilized Gold Nanoparticles, ChemCatChem, 8 (2016) 3121-3130.

[17] H. Kitahara, H. Sakurai, Catalytic activity of gold nanoclusters in intramolecular hydroamination of alkenes and alkynes with toluenesulfonamide under aerobic and basic conditions, J. Organomet. Chem., 696 (2011) 442-449.

[18] A. Corma, P. Concepción, I. Domínguez, V. Forné, M.J. Sabater, Gold supported on a biopolymer (chitosan) catalyzes the regioselective hydroamination of alkynes, J. Catal., 251 (2007) 39-47.

[19] D. Liu, Q. Nie, R. Zhang, M. Cai, Regiospecific Hydroamination of Unsymmetrical Electron-Rich and Electron-Poor Alkynes with Anilines Catalyzed by Gold(I) Immobilized in MCM-41, Adv. Synth. Catal., 360 (2018) 3940-3948.

[20] A. Zambelli, M. Caprio, A. Grassi, D.E. Bowen, Syndiotactic styrene-butadiene block copolymers synthesized with CpTiX3/MAO (Cp = C5H5, X = Cl, F; Cp = C5Me5, X = Me) and TiXn/MAO (n = 3, X = acac; n = 4, X = O-tert-Bu), Macromol. Chem. Phys., 201 (2000) 393-400.

[21] A. Buonerba, C. Cuomo, V. Speranza, A. Grassi, Crystalline Syndiotactic Polystyrene as Reinforcing Agent of cis-1,4-Polybutadiene Rubber, Macromolecules, 43 (2010) 367-374.

[22] A. Buonerba, V. Speranza, P. Canton, C. Capacchione, S. Milione, A. Grassi, Novel nanostructured semicrystalline ionomers by chemoselective sulfonation of multiblock copolymers of syndiotactic polystyrene with polybutadiene, RSC Adv., 4 (2014) 60158-60167.

[23] A. Buonerba, M. Fienga, S. Milione, C. Cuomo, A. Grassi, A. Proto, C. Capacchione, Binary Copolymerization of p-Methylstyrene with Butadiene and Isoprene Catalyzed by Titanium Compounds Showing Different Stereoselectivity, Macromolecules, 46 (2013) 8449-8457.

[24] A. Buonerba, F.D. Monica, V. Speranza, C. Capacchione, S. Milione, A. Grassi, Thin-film nanostructure and polymer architecture in semicrystalline syndiotactic poly(p-methylstyrene)–(cis-1,4-polybutadiene) multiblock copolymers, Polym. Int., 68 (2019) 1681-1687.

[25] G. Guerra, C. Daniel, P. Rizzo, O. Tarallo, Advanced materials based on polymer cocrystalline forms, J. Polym. Sci., Part B: Polym. Phys., 50 (2012) 305-322.

[26] G. Milano, G. Guerra, Understanding at molecular level of nanoporous and co-crystalline materials based on syndiotactic polystyrene, Prog. Mater Sci., 54 (2009) 68-88.

[27] E.B. Gowd, K. Tashiro, C. Ramesh, Structural phase transitions of syndiotactic polystyrene, Prog. Polym. Sci., 34 (2009) 280-315.

[28] M. Malanga, Syndiotactic Polystyrene Materials, Adv. Mater., 12 (2000) 1869-1872.

[29] G. Guerra, A.R. Albunia, C. D'Aniello, Preparation, Structure, Properties, and Applications of Co-Crystals and Nanoporous Crystalline Phases of Syndiotactic Polystyrene, in: J. Schellenberg (Ed.) Syndiotactic Polystyrene, John Wiley & Sons, Inc, Hoboken, New Jersey, 2009, pp. 194-237.

[30] A. Buonerba, C. Cuomo, S. Ortega Sánchez, P. Canton, A. Grassi, Gold Nanoparticles Incarcerated in Nanoporous Syndiotactic Polystyrene Matrices as New and Efficient Catalysts for Alcohol Oxidations, Chem. Eur. J., 18 (2012) 709-715.

[31] A. Buonerba, S. Impemba, A.D. Litta, C. Capacchione, S. Milione, A. Grassi, Aerobic Oxidation and Oxidative Esterification of 5-Hydroxymethylfurfural by Gold Nanoparticles Supported on Nanoporous Polymer Host Matrix, ChemSusChem, 11 (2018) 3139-3149.

[32] A. Buonerba, A. Noschese, A. Grassi, Highly Efficient Direct Aerobic Oxidative Esterification of Cinnamyl Alcohol with Alkyl Alcohols Catalysed by Gold Nanoparticles Incarcerated in a Nanoporous Polymer Matrix: A Tool for Investigating the Role of the Polymer Host, Chem. Eur. J., 20 (2014) 5478-5486.

[33] A. Noschese, A. Buonerba, P. Canton, S. Milione, C. Capacchione, A. Grassi, Highly efficient and selective reduction of nitroarenes into anilines catalyzed by gold nanoparticles incarcerated in a nanoporous polymer matrix: Role of the polymeric support and insight into the reaction mechanism, J. Catal., 340 (2016) 30-40.

[34] R.J. Batrice, M.S. Eisen, Catalytic insertion of E–H bonds (E = C, N, P, S) into heterocumulenes by amido–actinide complexes, Chem. Sci., 7 (2016) 939-944.

[35] A. Tillack, V. Khedkar, H. Jiao, M. Beller, A General Study of Aryloxo and Alkoxo Ligands in the Titanium-Catalyzed Intermolecular Hydroamination of Terminal Alkynes, Eur. J. Org. Chem., 2005 (2005) 5001-5012.

[36] W. Li, G. Hou, M. Chang, X. Zhang, Highly Efficient and Enantioselective Iridium-Catalyzed Asymmetric Hydrogenation of N-Arylimines, Adv. Synth. Catal., 351 (2009) 3123-3127.

[37] Z. Han, Z. Wang, X. Zhang, K. Ding, Spiro[4,4]-1,6-nonadiene-Based Phosphine–Oxazoline Ligands for Iridium-Catalyzed Enantioselective Hydrogenation of Ketimines, Angew. Chem. Int. Ed., 48 (2009) 5345-5349.

[38] A. Buonerba, R. Lapenta, A. Donniacuo, M. Licasale, E. Vezzoli, S. Milione, C. Capacchione, M.F. Tecce, A. Falqui, R. Piacentini, C. Grassi, A. Grassi, NIR multiphoton ablation of cancer cells, fluorescence quenching and cellular uptake of dansyl-glutathione-coated gold nanoparticles, Sci. Rep., 10 (2020) 11380.

[39] M.J. Frisch, G.W. Trucks, H.B. Schlegel, G.E. Scuseria, M.A. Robb, J.R. Cheeseman, G. Scalmani, V. Barone, G.A. Petersson, H. Nakatsuji, X. Li, M. Caricato, A.V. Marenich, J. Bloino, B.G. Janesko, R. Gomperts, B. Mennucci, H.P. Hratchian, J.V. Ortiz, A.F. Izmaylov, J.L. Sonnenberg, D. Williams-Young, F. Ding, F. Lipparini, F. Egidi, J. Goings, B. Peng, A. Petrone, T. Henderson, D. Ranasinghe, V.G. Zakrzewski, J. Gao, N. Rega, G. Zheng, W. Liang, M. Hada, M. Ehara, K. Toyota, R. Fukuda, J. Hasegawa, M. Ishida, T. Nakajima, Y. Honda, O. Kitao, H. Nakai, T. Vreven, K. Throssell, J.A. Montgomery, Jr., J.E. Peralta, F. Ogliaro, M.J. Bearpark, J.J. Heyd, E.N. Brothers, K.N. Kudin, V.N. Staroverov, T.A. Keith, R. Kobayashi, J. Normand, K. Raghavachari, A.P. Rendell, J.C. Burant, S.S. Iyengar, J. Tomasi, M. Cossi, J.M. Millam, M.

Klene, C. Adamo, R. Cammi, J.W. Ochterski, R.L. Martin, K. Morokuma, O. Farkas, J.B. Foresman, D.J. Fox, Gaussian 16, Revision C.01, Gaussian, Inc., , Wallingford CT, 2016.

[40] J.P. Perdew, K. Burke, M. Ernzerhof, Generalized Gradient Approximation Made Simple, Phys. Rev. Lett., 77 (1996) 3865-3868.

[41] F. Weigend, R. Ahlrichs, Balanced basis sets of split valence, triple zeta valence and quadruple zeta valence quality for H to Rn: Design and assessment of accuracy, PCCP, 7 (2005) 3297-3305.

[42] J. Cordón, G. Jiménez-Osés, J.M. López-de-Luzuriaga, M. Monge, The key role of Au-substrate interactions in catalytic gold subnanoclusters, Nat, Commun., 8 (2017) 1657.

[43] S. Grimme, S. Ehrlich, L. Goerigk, Effect of the damping function in dispersion corrected density functional theory, J. Comput. Chem., 32 (2011) 1456-1465.

[44] A. Todd, T.K. Keith, AIMAll (Version 19.10.12), Gristmill Software, Overland Park KS, USA, 2019.

[45] A. Corma, A. Leyva-Pérez, M.J. Sabater, Gold-Catalyzed Carbon−Heteroatom Bond-Forming Reactions, Chem. Rev., 111 (2011) 1657-1712.

[46] Y. Miyazaki, S. Kobayashi, Novel Gold(III) Polymer-Supported Catalyst for Indole Library Synthesis, J. Comb. Chem., 10 (2008) 355-357.

[47] J. Sá, A. Goguet, S.F.R. Taylor, R. Tiruvalam, C.J. Kiely, M. Nachtegaal, G.J. Hutchings, C. Hardacre, Influence of Methyl Halide Treatment on Gold Nanoparticles Supported on Activated Carbon, Angew. Chem. Int. Ed., 50 (2011) 8912-8916.

[48] A. Couce-Rios, G. Kovács, G. Ujaque, A. Lledós, Hydroamination of C–C Multiple Bonds with Hydrazine Catalyzed by N-Heterocyclic Carbene–Gold(I) Complexes: Substrate and Ligand Effects, ACS Catal., 5 (2015) 815-829.

[49] J. Mielke, F. Leyssner, M. Koch, S. Meyer, Y. Luo, S. Selvanathan, R. Haag, P. Tegeder, L. Grill, Imine Derivatives on Au(111): Evidence for "Inverted" Thermal Isomerization, ACS Nano, 5 (2011) 2090-2097.

[50] A. Zhdanko, M.E. Maier, Mechanistic Study of Gold(I)-Catalyzed Hydroamination of Alkynes: Outer or Inner Sphere Mechanism?, Angew. Chem. Int. Ed., 53 (2014) 7760-7764.